small methods
www.small-methods.com

Exceptional Stability against Water, UV Light, and Heat for $CsPbBr_3$@Pb-MOF Composites

Chenxu Wang, Lihe Yan, Jinhai Si,* Ning Wang, Ting Li, and Xun Hou*

All-inorganic lead halide perovskite nanocrystals (NCs) have been widely applied in optoelectronic devices owing to their excellent photoluminescence (PL) properties. However, poor stability upon exposure to water, UV light or heat strongly limits their practical application. Herein, $CsPbBr_3$@Pb-MOF composites with exceptional stability against water, UV light, and heat are synthesized by ultrasonic processing the precursors of lead-based MOF (Pb-MOF), oleylammonium bromide (OAmBr) and cesium oleate (Cs-OA) solutions at room temperature. Pb-MOF can not only provide the lead source for the in situ growth of $CsPbBr_3$ NCs, but also the protective layer of perovskites NCs. The formed $CsPbBr_3$@Pb-MOF composites show a considerable PL quantum yield (PLQY) of 67.8%, and can maintain 90% of the initial PL intensity when immersed in water for 2 months. In addition, the outstanding PL stability against UV light and heat is demonstrated with $CsPbBr_3$ NCs synthesized by the conventional method as a comparison. Finally, a green (light-emitting diode) LED is fabricated using green-emitting $CsPbBr_3$@Pb-MOF composites and exhibits excellent stability without packaging when immersed in water for 30 days. This study provides a practical approach to improve the stability in aqueous phase, which may pave the way for future applications for various optoelectronic devices.

1. Introduction

All-inorganic $CsPbX_3$ (X = Cl, Br, I) perovskite nanocrystals (NCs) have emerged as ideal semiconducting alternatives in various optoelectronic applications, such as solar cells,[1–3] light-emitting diodes (LEDs),[4,5] photodetectors,[6,7] lasers[8,9] and so on[10–12] owing to their high absorption coefficients, narrow emission line width, tunable wavelength (400–700 nm), high photoluminescence quantum yield (PLQY), and low-cost synthesis processes.[13,14] Despite their giant application potential, the inherent susceptibility to extrinsically induced degradation toward polar solvents, oxygen, heat, and UV light limited their widespread commercialization seriously.[15–18] Especially, they would lose their structural integrity and emission ability when exposed to aqueous medium or even in humid air, which could be due to the ionic character of $CsPbX_3$ NCs along with their fragile surfaces and metastable structures.[19] Therefore, overcoming the instability of NCs has been a top priority and enormous efforts have been devoted to stabilizing perovskite NCs by functionalizing them with moisture-tolerance molecules,[20–24] depositing passivation layers[25] and so on.[26–28] Especially, various of encapsulation strategies including polymer coatings,[29–31] inorganic oxides,[32–35] solid or mesoporous silica,[36–38] shell formation[39–42] have been explored.

Recently, metal-organic frameworks (MOFs) have been used to protect the perovskites NCs,[43–46] owing to their simple preparation process, high specific surface area, and of particular interest is the capability for tunable of structural and coordination metal.[38,47] MOFs are constructed from intramolecular pores self-assembled by organic ligands and metal ions through coordination bonds.[48] Hou et al reported a family of scalable composites fabricated through liquid-phase sintering of perovskites and MOFs glasses. The processable composites showed high stability against immersion in water and organic solvents as well as exposure to heat, light, air, and ambient humidity.[45] Lian et al demonstrated a $CsPbBr_3$/ZIF-62 composite that could exhibit high stability against polar solvents, heat, light, and ambient humidity by sintering of ZIF-62 in air at ≈300 °C to completely seal the perovskite within the insulating matrix.[49] However, the preparation methods were complicated and always accompanied by high-temperature sintering, which could induce the agglomeration of perovskites NCs and lead to the fluorescence quenching. Hence, it is challenging to realize the preparation of perovskites NCs inside MOFs through a facile synthesis and gain improved stability against water, light, and heat.[43,50]

Herein, $CsPbBr_3$@Pb-MOF composites with exceptional stability underwater, UV light, and heat in water were synthesized by ultrasonic processing the precursors of lead-based MOF (Pb-MOF), oleylammonium bromide (OAmBr) and Cs-OA solutions at room temperature. Pb-MOF could not only provide the lead source for the in-situ growth of $CsPbBr_3$ NCs, but also the

C. Wang, L. Yan, J. Si, N. Wang, T. Li, X. Hou
Key Laboratory for Physical Electronics and Devices of the Ministry of Education and Shaanxi Key Laboratory of Photonics Technology for Information
School of Electronic Science and Engineering
Xi'an Jiaotong University
No.28, Xianning West Road, Xi'an 710049, China
E-mail: liheyan@mail.xjtu.edu.cn; jinhaisi@mail.xjtu.edu.cn

The ORCID identification number(s) for the author(s) of this article can be found under https://doi.org/10.1002/smtd.202400241

DOI: 10.1002/smtd.202400241

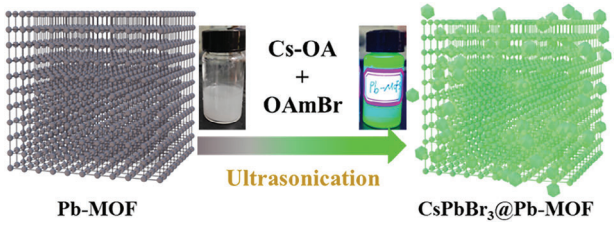

Figure 1. Schematic of the preparation of $CsPbBr_3$@Pb-MOF composites.

protective layer of perovskites NCs. The formed $CsPbBr_3$@Pb-MOF composites showed a considerable PLQY of 67.8%, and the long-term stability against water, UV light, and heat was demonstrated with $CsPbBr_3$ NCs synthesized by the conventional method as a comparison. Finally, green LED was fabricated using green-emitting $CsPbBr_3$@Pb-MOF composites and exhibited excellent stability in water without package.

2. Results and Discussion

2.1. Synthesis of CsPbBr3@Pb-MOF Composites

The $CsPbBr_3$@Pb-MOF composites were synthesized by ultrasonic and $CsPbBr_3$-HI NCs were synthesized using the conventional hot injection(HI) method (see details in the Supporting Information).[51] The Pb-MOF ($(Pb_2(1,3,5\text{-}HBTC)_2(H2O)_4$, see Figure S1, Supporting Information) was prepared using a self-assembly method by dissolving lead (II) acetate trihydrate and 1,3,5-H_3BTC_2 in the aqueous solution according to Sadeghzadeh's report.[52] In the specific synthesis, oily-liquid OAmBr and Cs-OA were prefabricated and well dispersed in hexane. Pb-MOF powders, Cs-OA, and OAmBr were added into hexane to grow $CsPbBr_3$ NCs in Pb-MOF, and $CsPbBr_3$@Pb-MOF composites were formed in situ. The synthesis process diagram is shown in **Figure 1**.

Scanning electron microscopy (SEM) was used to characterize the morphology and elements of the products, as shown in **Figures** 2a,b, and S2 (Supporting Information). The morphology of composites showed a micron rod shape with some attached flaky materials. Combined with the SEM of Pb-MOF (Figure S1, Supporting Information), the micron rod was Pb-MOF and the flaky materials might be isolated $CsPbBr_3$ NCs distributed outside or the broken Pb-MOF. Energy dispersive spectroscopy (EDS) showed that not only the Pb element but also Cs and Br elements in the composites were observed and they could correspond well with the distribution of crystals. Further, transmission electron microscopy (TEM) was characterized to test the morphology, distribution and fine structure of $CsPbBr_3$ NCs for the composites. As shown in Figure 2c, only MOF rod structures could be observed for the product at low magnification TEM. By selecting and enlarging the MOF rod (Figure 2d), $CsPbBr_3$ NCs with a size of ≈ 15 nm distributed well in Pb-MOF crystals could be observed. The high-resolution transmission electron microscopy (HRTEM, Figure 2e) and the fast Fourier transformation (FFT) images (Figure 2f) showed that the NCs had a high crystal quality with the lattice fringes of 0.58 and 0.41 nm, corresponding to the (100) and (110) crystal faces of the $CsPbBr_3$ crystal,[51,53] respectively.

In order to explore the fluence of the ratio of Cs and Br precursor on the morphology and PL characteristics of the sample, the ratio of the two was changed from 1: 10 (20 µL for Cs-OA) to 9: 10 (180 µL for Cs-OA). The photoluminescence (PL) photographs of crude solution for different ratios are shown in Figure 2g. It could be seen that with the increase of the proportion, the PL changed from blue to green light. To obtain the morphology of the samples, the supernatant and precipitation with 60, 100, and 180 µL for Cs-OA were characterized by TEM and shown in Figure S4 (Supporting Information) and Figure 2c–f. Monodispersed $CsPbBr_3$ NCs with a size less than 10 nm were shown in the supernatant for 60 µL Cs-OA; as for 100 and 180 µL, there were larger and more uneven rod-like materials. In the TEM analysis of the precipitation, 60 µL Cs-OA revealed intact Pb-MOF with attached nanoplates (NPLs) and did not find $CsPbBr_3$ NCs within the Pb-MOF. At 100 µL, the Pb-MOF retained their shapes, and $CsPbBr_3$ NCs with a size of ≈ 15 nm distributed well in Pb-MOF crystals. With 180 µL, the MOF was fragmented with reduced size. There were some aggregated $CsPbBr_3$ NCs with a size of 50 nm surrounding the Pb-MOF.

Meanwhile, PL spectra of supernatant and precipitation under different proportions were shown in Figure S3 (Supporting Information) and Figure 2h. From the Figure, we found that with the increase of the proportion, the PL of the sample would redshift, indicating the increase size of the $CsPbBr_3$ NCs. The supernatant of samples with 60 µL for Cs-OA had the highest PL intensity at 508 nm, which could be attributed to the generation of small and monodispersed $CsPbBr_3$ NCs. As for 100 and 180 µL, owing to the larger size of $CsPbBr_3$ NCs shown in the TEM, they had a weak PL intensity with red-shifted PL wavelength. In addition to the PL peak of $CsPbBr_3$ NCs at 509 nm, there was an additional weak PL peak at 435 nm in the precipitation for sample with 60 µL for Cs-OA, which can be attributed to 2-layer $CsPbBr_3$ NPLs by combining with TEM images.[54] The PL wavelength of high proportions were redshifted to 526 nm and 100 µL showed highest PL intensity. The highest PL intensity could be owing to that $CsPbBr_3$ NCs with size of 15 nm were well-distributed in Pb-MOF crystals for 100 µL Cs-OA. While for 140 and 180 µL, the PL property of $CsPbBr_3$ NCs were reduced seriously owing to their agglomeration. Furthermore, fluorescence confocal microscope measurement was used to further demonstrated the PL origin of the samples for 3: 10 (60 µL for Cs-OA) and 5: 10 (100 µL for Cs-OA), as shown in Figure S5 (Supporting Information). The PL of a sample prepared using 60 µL Cs-OA was concentrated in the solution phase, while for 100 µL Cs-OA, the PL originated mainly from the MOF rods. Therefore, 100 µL Cs-OA was selected as the optimal ratio for the preparation of the sample and its further characterizations. Notably, PLQY of the prepared $CsPbBr_3$@Pb-MOF composites (Figure S6, Supporting Information) were measured to be 67.8%, which was even higher than $CsPbBr_3$-HI NCs (55%). The outstanding PLQY for $CsPbBr_3$@Pb-MOF composites could be attributed to the passivation of defects by the Pb-MOF.

2.2. Water and Long-Term Stability

The prepared $CsPbBr_3$@Pb-MOF composites in hexane were centrifuged to obtain the powder sample (MOF-H). MOF-H

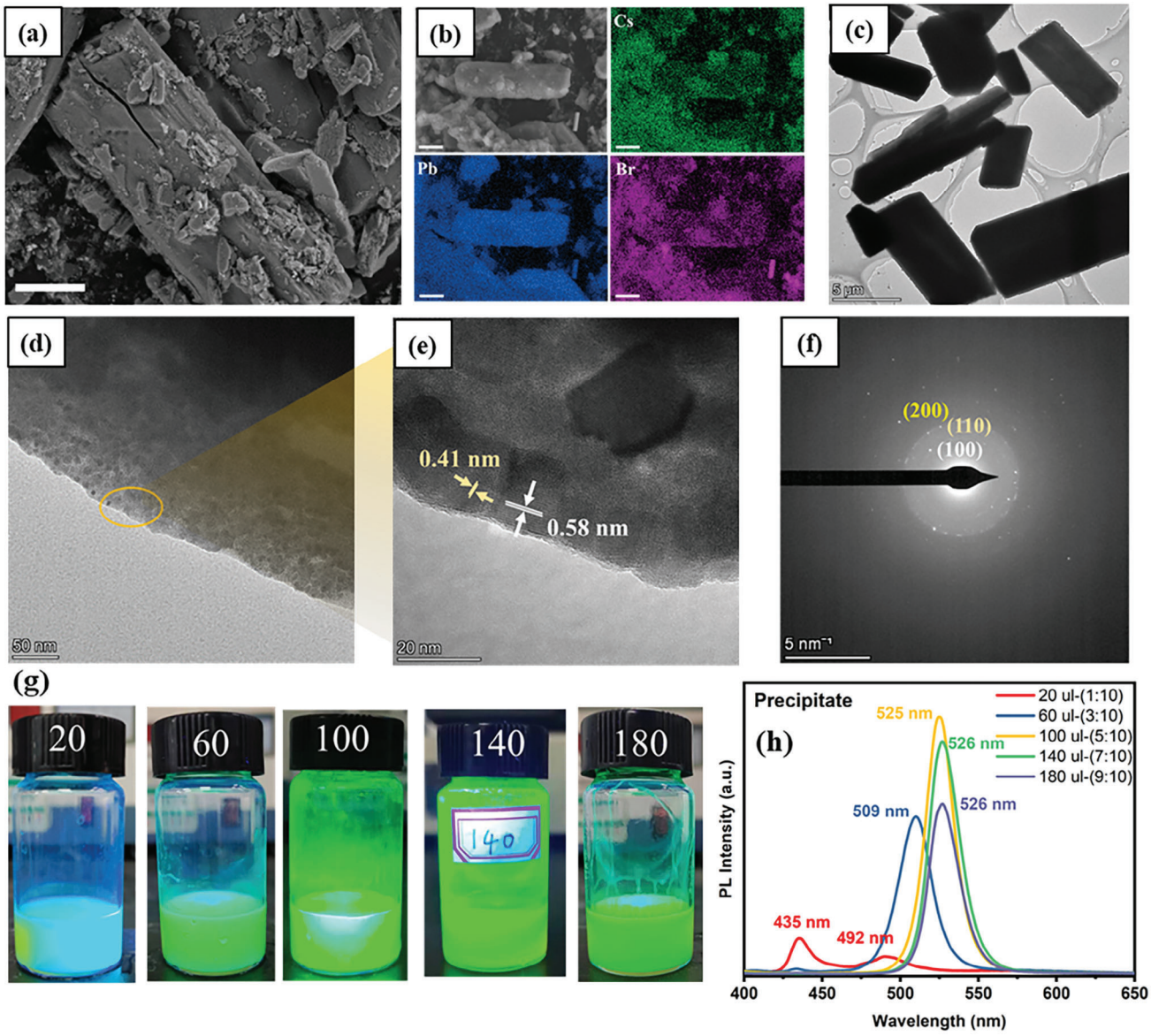

Figure 2. a,b) SEM micrograph and EDS mapping of $CsPbBr_3$@Pb-MOF composites; Scale bar: 2 μm. c–e) TEM and HRTEM micrographs of $CsPbBr_3$@Pb-MOF composites. f) The FFT image of e). g,h) The (g) photographs and PL properties of (h) precipitate for $CsPbBr_3$@Pb-MOF composites under different ratios of Cs and Br precursor.

powder was then sequentially processed by ethanol and water, and then the powder samples, namely MOF-E and MOF-W, were obtained by centrifugation. The optical images under ambient and 365 nm UV light of MOF-H, MOF-E, and MOF-W powders were shown by the insets of **Figure** 3a. MOF-H and MOF-E powders showed a yellow color, which is the typical color of $CsPbBr_3$ perovskite NCs. MOF-W powder showed a white color, being similar with the color of Pb-MOF. The three powders could emit strong green fluorescence under UV light. As a contrast, the same treatment was carried out on the NCs prepared by the HI method and the samples were named as HI-H, HI-E, and HI-W, respectively. As shown in Figure 3a, MOF-E and MOF-W could achieve 80% and 30% of the PL intensity of MOF-H respectively, which were much stronger than those of HI-E and HI-W (as given by Figure S7a, Supporting Information). Then, PL (under 400 nm excitation) and photoluminescence emission (PLE) spectra of the MOF-H and MOF-W composites were further measured. As shown in Figure 3b, MOF-H exhibited a green emission peak at 526 nm with 18 nm full-width-at-half maximum (FWHM) while MOF-W showed a blue-shifted emission peak at 518 nm and narrower FWHM of 16 nm. The reason for blue-shifted PL with narrower FWHM could be due to the degradation of $CsPbBr_3$ NCs on the surface of MOF. The PL originated from the NCs inside the MOF, and the distribution of $CsPbBr_3$ NCs was more uniform, and aggregation of the NCs could be avoided due to the isolation by the porous structure of Pb-MOF. Besides, the PLE spectrum showed a wide excitation wavelength for both samples, indicating the excellent absorption properties.[42]

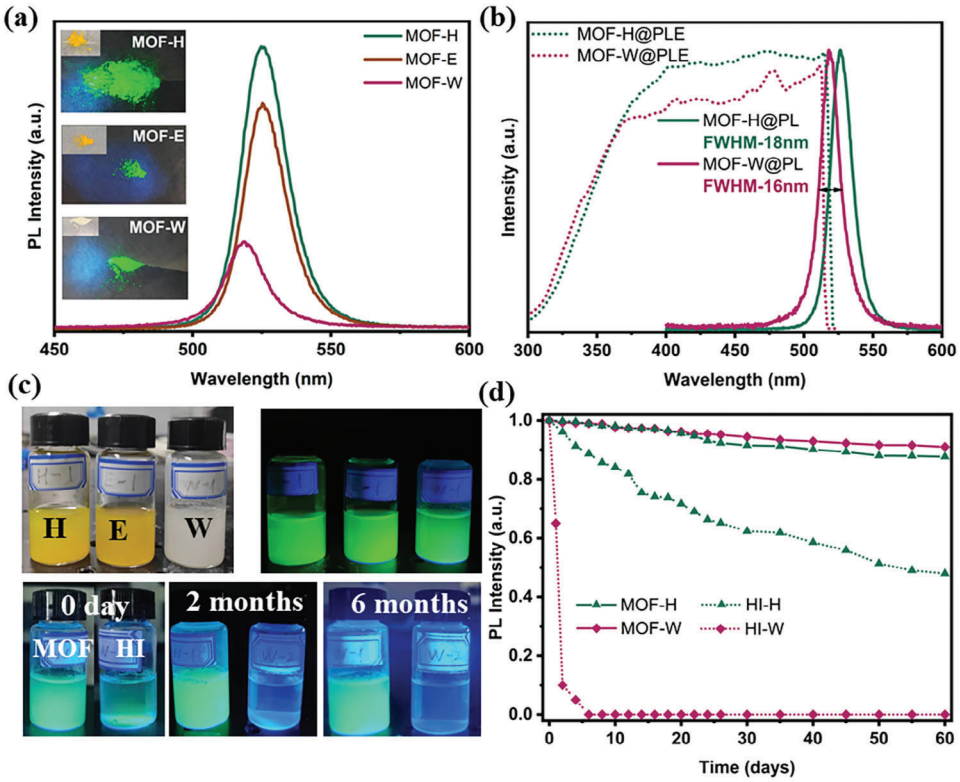

Figure 3. a) PL intensities of $CsPbBr_3$@Pb-MOF in hexane, ethanol, and water, the inset are the optical images of their powders under ambient light and 365 nm UV light. b) PL and PLE spectra of MOF-H and MOF-W, respectively. c) Optical images of samples (From left to right, that's in hexane, ethanol, and water) under ambient light and 365 nm UV light (upper) and optical images of samples $CsPbBr_3$@Pb-MOF (left) and $CsPbBr_3$-HI (right) in water for 0 day, 2 months and 6 months under 365 nm UV light (bottom). d) Long-term stability of $CsPbBr_3$@Pb-MOF and $CsPbBr_3$-HI in hexane and water.

The obtained samples were then dispersed in hexane, ethanol, and water, as shown in Figure 3c (upper) and Figure S7b (Supporting Information), respectively. The corresponding long-term PL intensity of the sample in hexane and water were characterized and shown in Figure 3d. It can be seen that whether it was dispersed in hexane or water, $CsPbBr_3$@Pb-MOF composites showed better long-term stability than conventional HI NCs. Unlike conventional HI NCs which would rapidly degrade in water and lose their PL properties, the $CsPbBr_3$@Pb-MOF composites still achieved over 90% of their initial PL intensity after immersing in water for 2 months. Optical images of $CsPbBr_3$@Pb-MOF and HI NCs immersed in water with long-term stability for 0 days, 2 months, and even 6 months under ambient light and 365 nm UV light were shown in Figure 3c (bottom), which indicated their extremely excellent stability in water and promising applications in aqueous phase.

2.3. Structure and Morphology Characterization

To reveal the reason for the good stability of the sample, a model of MOF-W composites was proposed and shown in the **Figure** 4a. First, the growth mechanism of the NCs was put forward by the in-situ PL spectra, as shown in Figure S8 (Supporting Information). Ultra-small $CsPbBr_3$ NCs were formed immediately with strong quantum confinement effect and showed blue PL under UV light at the beginning. With the increase of reaction time, the wavelength of PL redshifted with green fluorescence emitting owing to the $CsPbBr_3$ NCs became larger. This occurs due to the reduced potential barrier for Cs and Br precursors to enter the MOF under ultrasonic conditions and considerable $CsPbBr_3$ NCs generated by reaction with the Pb both inside and on the surface of Pb-MOF. The prepared sample was call $CsPbBr_3$@Pb-MOF-H.

Due to the ionic properties of perovskite, water would induce the dissolution of NCs and larger grains could be formed by recrystallization, resulting in the reduction of PL properties.[55,56] The NCs on the surface of Pb-MOF would be degraded after the treatment of water, while the internal NCs could be effectively reserved owing to the encapsulation of the MOF framework(called $CsPbBr_3$@Pb-MOF-W). The density of the NCs would reduce owing to the degradation of the surface NCs, which could correspond to the PL of the composites blue-shifted from 526 to 518 nm, as shown by the PL spectra given in Figure 3b. Meanwhile, the contact area between the inner NCs and water would be reduced owing to the protection of the framework. The confined Pb-MOF interior and the hydrophobic surface ligands could effectively prevent moisture from entering and the $CsPbBr_3$ NCs could survive when immersing in water for a long time.[57,58]

X-ray diffraction (XRD), X-ray photoelectron spectroscopy (XPS), and SEM were used to further verify the structure (as given

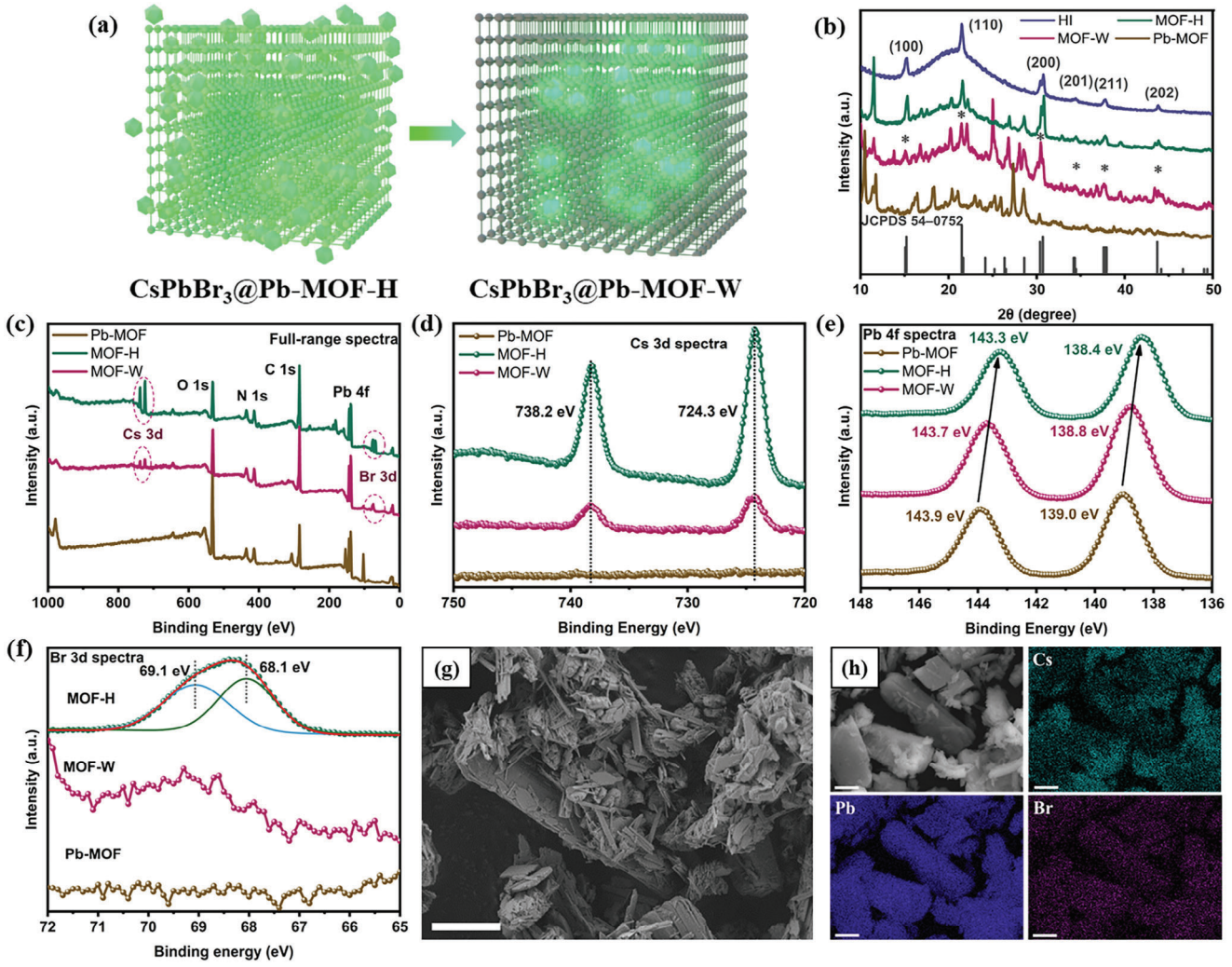

Figure 4. a) Schematic of MOF-H and MOF-W. b) XRD patterns of $CsPbBr_3$-HI, Pb-MOF, MOF-H, and MOF-W. c–f) XPS spectra of the Pb-MOF, MOF-H, and MOF-W: c) the full-range spectra; d) Cs 3d spectra; e) Pb 4f spectra; f) Br 3d spectra. g) SEM micrograph of MOF-W and h) EDS mapping images; Scale bar: 2 μm.

in Figure 4). Compared with the $CsPbBr_3$ NCs prepared by HI method, MOF-H, and MOF-W composites also showed obvious diffraction peaks of $CsPbBr_3$ (Mark by *, Figure 4b).[53] XPS measurements were performed to examine chemical elements. As shown in the full-range XPS spectra (Figure 4c), the signals of Cs and Br elements appeared in both MOF-H and MOF-W composites. According to the high resolved spectra for Cs 3d (Figure 4d), two peaks centered at 738.2 and 724.3 eV owing to Cs $3d_{3/2}$ and Cs $3d_{5/2}$ were observed in MOF-H and MOF-W composites. Moreover, compared with the Pb-MOF, the Pb 4f peaks shift to lower binding energies (from 143.9 to 143.2 eV, from 139.0 to 138.3 eV, shown in Figure 4e) and slightly broaden for the MOF-H composites, suggesting the change of coordination chemistry of Pb atoms (the emerging Pb–Br bond from $CsPbBr_3$ NCs).[41] The binding energies of the Pb 4f peaks of the MOF-W were 143.7 and 138.8 eV, respectively, which were between those of Pb-MOF and MOF-H, indicating that although part of the $CsPbBr_3$ NCs were degraded after water treatment, some of the NCs were still protected by MOF and made the binding energy still lower than Pb-MOF. By further fitting the Br 3d spectra for MOF-H (Figure 4f), the peaks centered at 69.1 and 68.1 eV were attributed to Br $3d_{3/2}$ and $3d_{5/2}$, respectively. Because XPS could only obtain elemental information for the surface states (<10 nm) and couldn't detect the deeper signal, the intensity of Br 3d spectra in MOF-W was very weak. SEM and EDS mapping were used to characterize the morphology and element distribution of the samples, as shown in Figure 4f,g. Element distribution showed that Cs, Pb, and Br were distributed along the MOF rod, indicating that the $CsPbBr_3$ NCs were wrapped in the MOF rod. The distribution and atomic ratio of elements at different depths were characterized by changing the voltage of EDS. When the voltage was increased from 10 to 20 kV, detection depth was increased, and the ratio of Br: Pb elements increased from 0.26: 15.87 to 0.33: 10.99 (Table S1, Supporting Information), further indicating the existence of $CsPbBr_3$ NCs inside the MOF.

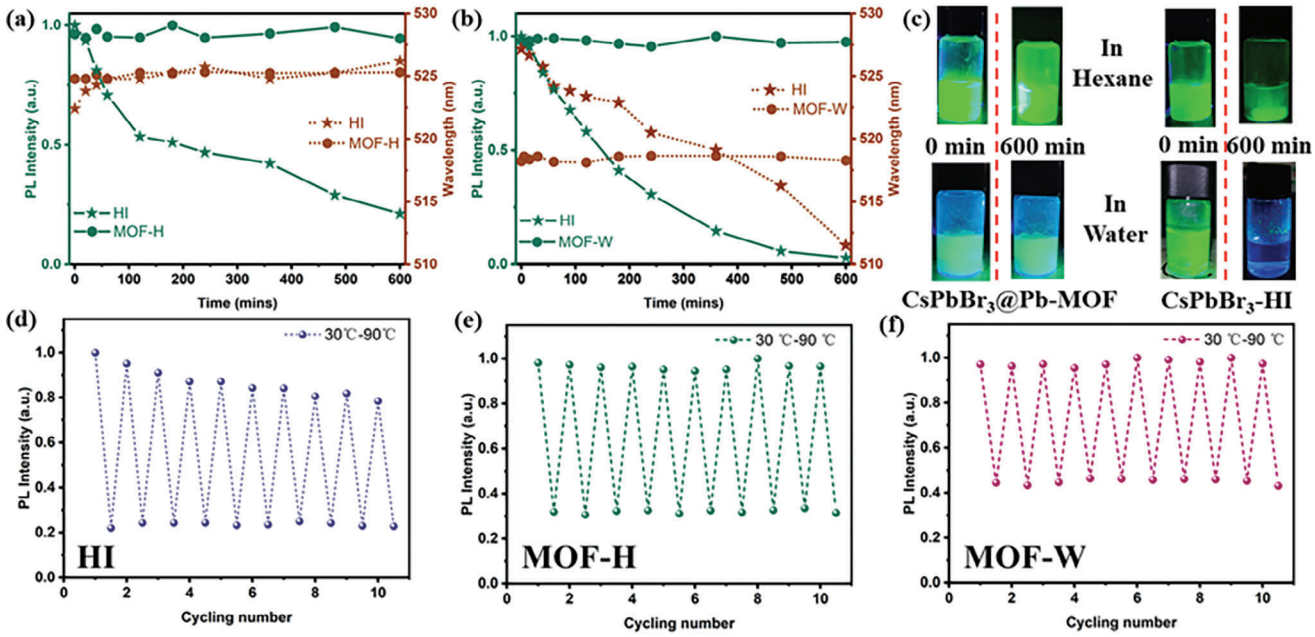

Figure 5. UV light stability of $CsPbBr_3$@Pb-MOF composites and $CsPbBr_3$-HI NCs in (a) hexane and (b) water. c) The optical PL images of 0 and 600 min radiation of UV light for $CsPbBr_3$@Pb-MOF composites (left) and $CsPbBr_3$-HI NCs (right) in hexane and water. d–f) Normalized PL intensity variations of d)$CsPbBr_3$-HI, e) MOF-H, and f) MOF-W going through 10 thermal cycles with the temperature varying between 30 and 90 °C.

2.4. UV Light and Heat Stability

Considering that perovskite NCs could suffer from UV light irradiation and ambient temperature change in practical application, UV light and heat stabilities of the prepared samples were characterized.[49,58] Here, the change of PL intensity and central wavelength of different samples were tested under continuous UV light irradiation in hexane and water, as shown in **Figure** 5a–c. The PL intensities and central wavelength of $CsPbBr_3$@Pb-MOF composites in hexane remained constant (Figure 5a; Figure S9a,b, Supporting Information) under 600 min of 365 nm UV irradiation. In contrast, for conventional $CsPbBr_3$-HI NCs, the surface ligands were removed by UV light and caused the agglomeration of NCs, causing the 80% reduction of the PL intensity as well as the redshift. Furthermore, $CsPbBr_3$@Pb-MOF composites in water showed an outstanding resistance (Figure 5b; Figure S9c,d, Supporting Information) when suffering the irradiation of 365 nm UV light. The optical PL images of the UV irradiation process of UV light for $CsPbBr_3$@Pb-MOF composites (left) and $CsPbBr_3$-HI NCs (right) in hexane and water are shown in Figure 5c.

The samples were then prepared on quartz glass plates by drop casting and the stability at high temperatures was tested. As shown in Figure S10a–c (Supporting Information), the raw PL intensity decreased with temperature rose from 30 to 90 °C. For $CsPbBr_3$-HI NCs, when the temperature rose to 90 °C, the PL intensity decreased to less than 20% of 30 °C, while for MOF-H composites, it could reach more than 30%. Surprisingly, MOF-W composites only dropped to 45% of 30 °C, which means better thermal stability after water treatment. Then, the cyclic stability of samples heating and cooling were characterized, as given in Figure 5d–f. The PL intensity of $CsPbBr_3$-HI NCs was constantly declining in the process of heating and cooling, which means the degradation of $CsPbBr_3$-HI NCs. For MOF-H and MOF-W composites, the outstanding PL characteristics could be maintained after 10 cycles, indicating that the perovskite NCs were well passivated from heat damage. The UV irradiation and heat treatment mainly destroy the surface of the $CsPbBr_3$ NCs. The surface ligands would undergo irreversible desorption and decomposition under UV irradiation and heat treatment, leading to the aggregation of $CsPbBr_3$ NCs and reducing their PL properties.[27,59] After the encapsulation of MOF framework, the surface ligands would be confined inside the MOF and the desorption would be reduced effectively with the inhibition of the of $CsPbBr_3$ NCs' aggregation.[60] To our knowledge, the preparation of $CsPbBr_3$ NCs with excellent PL stability in water, UV irradiation, and heat using such a simple method has not been reported elsewhere. Tables S2 and S3 (Supporting Information) summarize the synthesis methods and stability comparison of the reported MOF-based and some typical stable perovskite NCs with our work, respectively.

Given that the exceptional stability underwater, UV light, and heat for $CsPbBr_3$@Pb-MOF composites, green MOF-W@LED was fabricated using 445 nm commercial InGaN chip as backlight, as shown in **Figure** 6a respectively. The unpackaged LED were immersed in water and examined its emitting performance for 120 h, as shown in the Figure 6b,c. The MOF-W@LED still maintained excellent PL characteristics after being immersed in water for 120 h owing to the protection of the MOF framework. As shown in the inset of Figure 6c, even after 30 days, it still maintained excellent luminous properties.

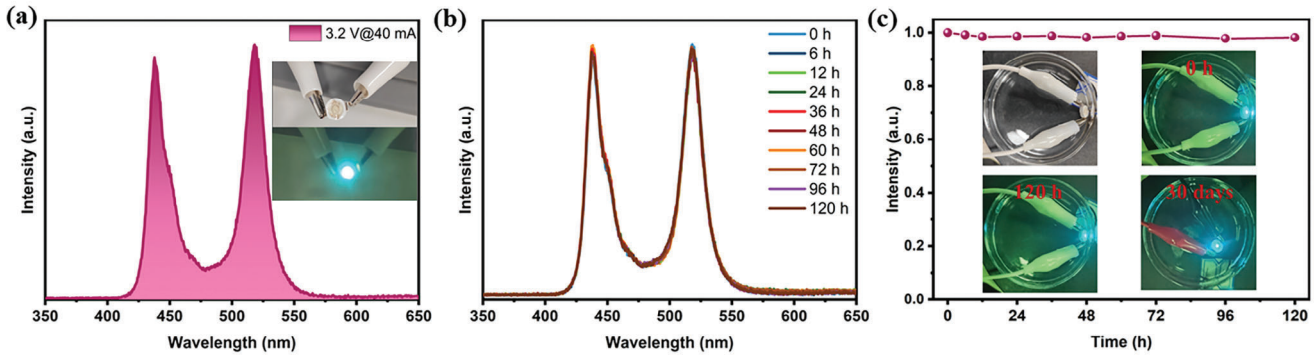

Figure 6. a) Green LED prepared by MOF-W composites. c) Long-term stability for MOF-W@LED immersed in water. d) Normalized PL intensity of MOF-W@LED; inset of (d) are the optical images of MOF-W@LED immersed in water for 0 h, 120 h, and 30 days.

3. Conclusion

In summary, $CsPbBr_3$@Pb-MOF composites with exceptional stability against water, UV light, and heat were synthesized by the ultrasonic method at room temperature. The formed $CsPbBr_3$@Pb-MOF composites showed a considerable PLQY of 67.8%, and could achieve 90% of the initial PL intensity when immersed in water for 2 months. In addition, the outstanding PL stability against UV light and heat were demonstrated with $CsPbBr_3$ NCs synthesized by the conventional method as a comparison. Finally, green LED was fabricated using green-emitting $CsPbBr_3$@Pb-MOF composites and exhibited excellent stability without packaged when immersed in water for 30 days. This study provides a practical approach to improve the stability of perovskite NCs in an aqueous phase, which may pave the way for future applications for various optoelectronic devices.

Supporting Information

Supporting Information is available from the Wiley Online Library or from the author.

Acknowledgements

The authors acknowledge the financial support from the National Natural Science Foundation of China (Grant No. 62027822) and the National Research and Development Program of China (Grant No. 2019YFA0706402).

Conflict of Interest

The authors declare no conflict of interest.

Data Availability Statement

The data that support the findings of this study are available from the corresponding author upon reasonable request.

Keywords

$CsPbBr_3$@Pb-MOF composites, encapsulation, heat stability, LED, UV light stability, water stability

Received: February 18, 2024
Revised: March 20, 2024
Published online:

[1] A. Swarnkar, A. R. Marshall, E. M. Sanehira, B. D. Chernomordik, D. T. Moore, J. A. Christians, T. Chakrabarti, J. M. Luther, *Science* **2016**, *354*, 92.
[2] W. Chi, S. K. Banerjee, *Angew. Chem., Int. Ed.* **2022**, *61*, 202112412.
[3] H. Aqoma, S.-H. Lee, I. F. Imran, J.-H. Hwang, S.-H. Lee, S.-Y. Jang, *Nat. Energy* **2024**, *9*, 324.
[4] J. Song, J. Li, X. Li, L. Xu, Y. Dong, H. Zeng, *Adv. Mater.* **2015**, *27*, 7162.
[5] Y. Jiang, C. Sun, J. Xu, S. Li, M. Cui, X. Fu, Y. Liu, Y. Liu, H. Wan, K. Wei, T. Zhou, W. Zhang, Y. Yang, J. Yang, C. Qin, S. Gao, J. Pan, Y. Liu, S. Hoogland, E. H. Sargent, J. Chen, M. Yuan, *Nature* **2022**, *612*, 679.
[6] P. Ramasamy, D. H. Lim, B. Kim, S. H. Lee, M. S. Lee, J. S. Lee, *Chem. Commun.* **2016**, *52*, 2067.
[7] C. Li, Y. Ma, Y. Xiao, L. Shen, L. Ding, *InfoMat* **2020**, *2*, 1247.
[8] S. Yakunin, L. Protesescu, F. Krieg, M. I. Bodnarchuk, G. Nedelcu, M. Humer, G. De Luca, M. Fiebig, W. Heiss, M. V. Kovalenko, *Nat. Commun.* **2015**, *6*, 8056.
[9] Y. Xu, Q. Chen, C. Zhang, R. Wang, H. Wu, X. Zhang, G. Xing, W. W. Yu, X. Wang, Y. Zhang, M. Xiao, *J. Am. Chem. Soc.* **2016**, *138*, 3761.
[10] H. Chen, L. Zhou, Z. Fang, S. Wang, T. Yang, L. Zhu, X. Hou, H. Wang, Z. L. Wang, *Adv. Funct. Mater.* **2021**, *31*, 2011073.
[11] Y. Xue, T. Yang, Y. Zheng, E. Wang, H. Wang, L. Zhu, Z. Du, X. Hou, K.-C. Chou, *J. Mater. Chem. A* **2022**, *10*, 21893.
[12] Y. Xue, T. Yang, Y. Zheng, K. Wang, E. Wang, H. Wang, L. Zhu, Z. Du, H. Wang, K. C. Chou, X. Hou, *Adv. Sci.* **2023**, *10*, 2300650.
[13] M. V. Kovalenko, L. Protesescu, M. I. Bodnarchuk, *Science* **2017**, *358*, 745.
[14] W. Shi, X. Zhang, C. Xie, H. S. Chen, P. Yang, *Adv. Opt. Mater.* **2023**, *12*, 2302129.
[15] X. Yuan, X. Hou, J. Li, C. Qu, W. Zhang, J. Zhao, H. Li, *Phys. Chem. Chem. Phys.* **2017**, *19*, 8934.
[16] H. Huang, M. I. Bodnarchuk, S. V. Kershaw, M. V. Kovalenko, A. L. Rogach, *ACS Energy Lett.* **2017**, *2*, 2071.
[17] D. Yang, X. Li, H. Zeng, *Adv. Mater. Interfaces* **2018**, *5*, 1701662.
[18] Y. Zhou, Y. Zhao, *Energy Environ. Sci.* **2019**, *12*, 1495.
[19] S. Cheng, H. Zhong, *J. Phys. Chem. Lett.* **2022**, *13*, 2281.
[20] Z. Li, Q. Hu, Z. Tan, Y. Yang, M. Leng, X. Liu, C. Ge, G. Niu, J. Tang, *ACS Appl. Mater. Interfaces* **2018**, *10*, 43915.
[21] H. Lian, W. Zhang, R. Zou, S. Gu, R. Kuang, Y. Zhu, X. Zhang, C. G. Ma, J. Wang, Y. Li, *Adv. Mater.* **2023**, *35*, 2304743.
[22] Y. Bai, M. Hao, S. Ding, P. Chen, L. Wang, *Adv. Mater.* **2021**, *34*, 2105958.

[23] K. Hills-Kimball, H. Yang, T. Cai, J. Wang, O. Chen, *Adv. Sci.* **2021**, *8*, 2100214.
[24] C. Xie, X. Zhang, H. S. Chen, P. Yang, *Small* **2023**, 2308896.
[25] A. Loiudice, S. Saris, E. Oveisi, D. T. L. Alexander, R. Buonsanti, *Angew. Chem., Int. Ed.* **2017**, *56*, 10696.
[26] Y. Wei, Z. Cheng, J. Lin, *Chem. Soc. Rev.* **2019**, *48*, 310.
[27] W. Lv, L. Li, M. Xu, J. Hong, X. Tang, L. Xu, Y. Wu, R. Zhu, R. Chen, W. Huang, *Adv. Mater.* **2019**, *31*, 1900682.
[28] X. Zhang, P. Yang, *Langmuir* **2023**, *39*, 11188.
[29] H. Huang, B. Chen, Z. Wang, T. F. Hung, A. S. Susha, H. Zhong, A. L. Rogach, *Chem. Sci.* **2016**, *7*, 5699.
[30] A. F. Carrizo, G. K. Belmonte, F. S. Santos, C. W. Backes, G. B. Strapasson, L. C. Schmidt, F. S. Rodembusch, D. E. Weibel, *ACS Appl. Mater. Interfaces* **2021**, *13*, 59252.
[31] J. Chen, X. Huang, Z. Xu, Y. Chi, *ACS Appl. Mater. Interfaces* **2022**, *13*, 33703.
[32] S. Huang, Z. Li, L. Kong, N. Zhu, A. Shan, L. Li, *J. Am. Chem. Soc.* **2016**, *138*, 5749.
[33] S. Li, D. Lei, W. Ren, X. Guo, S. Wu, Y. Zhu, A. L. Rogach, M. Chhowalla, A. K. Jen, *Nat. Commun.* **2020**, *11*, 1192.
[34] J. He, X. Zhang, C. Xie, H. S. Chen, P. Yang, *J. Mater. Chem. C* **2023**, *11*, 7654.
[35] Y. Zhan, Y. Liu, Q. Che, P. Yang, *ACS Appl. Nano Mater.* **2022**, *5*, 18645.
[36] H. C. Wang, S. Y. Lin, A. C. Tang, B. P. Singh, H. C. Tong, C. Y. Chen, Y. C. Lee, T. L. Tsai, R. S. Liu, *Angew. Chem., Int. Ed.* **2016**, *55*, 7924.
[37] Q. Zhang, B. Wang, W. Zheng, L. Kong, Q. Wan, C. Zhang, Z. Li, X. Cao, M. Liu, L. Li, *Nat. Commun.* **2020**, *11*, 31.
[38] X. Ren, Y. Zhai, P. Wang, Z. Xu, S. Gao, X. Chen, Q. Gu, B. Wang, J. Li, S. F. Liu, J. Yu, *Adv. Mater.* **2023**, *35*, 2301166.
[39] Q. Zhong, M. Cao, H. Hu, D. Yang, M. Chen, P. Li, L. Wu, Q. Zhang, *ACS Nano* **2018**, *12*, 8579.
[40] K. K. Liu, Q. Liu, D. W. Yang, Y. C. Liang, L. Z. Sui, J. Y. Wei, G. W. Xue, W. B. Zhao, X. Y. Wu, L. Dong, C. X. Shan, *Light Sci. Appl.* **2020**, *9*, 44.
[41] V. K. Ravi, S. Saikia, S. Yadav, V. V. Nawale, A. Nag, *ACS Energy Lett.* **2020**, *5*, 1794.
[42] C. Wang, L. Yan, J. Si, T. Huo, X. Hou, *J. Alloys Compd.* **2023**, *946*, 169272.
[43] J. Hou, Z. Wang, P. Chen, V. Chen, A. K. Cheetham, L. Wang, *Angew. Chem., Int. Ed.* **2020**, *59*, 19434.
[44] G. Y. Qiao, D. Guan, S. Yuan, H. Rao, X. Chen, J. A. Wang, J. S. Qin, J. J. Xu, J. Yu, *J. Am. Chem. Soc.* **2021**, *143*, 14253.
[45] J. Hou, P. Chen, A. Shukla, A. Krajnc, T. Wang, X. Li, R. Doasa, L. H. G. Tizei, B. Chan, D. N. Johnstone, R. Lin, T. U. Schulli, I. Martens, D. Appadoo, M. S. Ari, Z. Wang, T. Wei, S. C. Lo, M. Lu, S. Li, E. B. Namdas, G. Mali, A. K. Cheetham, S. M. Collins, V. Chen, L. Wang, T. D. Bennett, *Science* **2021**, *374*, 621.
[46] Y. Zhan, Y. Liu, A. Zhang, P. Yang, *Langmuir* **2022**, *38*, 11121.
[47] L. Chen, R. Luque, Y. Li, *Chem. Soc. Rev.* **2017**, *46*, 4614.
[48] H.-C. Zhou, J. R. Long, O. M. Yaghi, *Chem. Rev.* **2012**, *112*, 673.
[49] Z.-D. Lian, B. Wang, Z.-S. Wu, H. Lin, S.-S. Yan, J.-L. Li, K. Zhang, Q.-G. Zeng, J.-C. Xu, S. Chen, S.-P. Wang, K. W. Ng, *ACS Appl. Nano Mater.* **2023**, *6*, 1808.
[50] C. Zhang, B. Wang, W. Li, S. Huang, L. Kong, Z. Li, L. Li, *Nat. Commun.* **2017**, *8*, 1138.
[51] L. Protesescu, S. Yakunin, M. I. Bodnarchuk, F. Krieg, R. Caputo, C. H. Hendon, R. X. Yang, A. Walsh, M. V. Kovalenko, *Nano Lett.* **2015**, *15*, 3692.
[52] H. Sadeghzadeh, A. Morsali, *J. Coord. Chem.* **2010**, *63*, 713.
[53] C. Wang, J. Si, L. Yan, T. Li, X. Hou, *J. Chem. Phys.* **2024**, *160*, 034704.
[54] Y. Bekenstein, B. A. Koscher, S. W. Eaton, P. Yang, A. P. Alivisatos, *J. Am. Chem. Soc.* **2015**, *137*, 16008.
[55] K. K. Bass, R. E. McAnally, S. Zhou, P. I. Djurovich, M. E. Thompson, B. C. Melot, *Chem. Commun.* **2014**, *50*, 15819.
[56] Y. Wei, X. Deng, Z. Xie, X. Cai, S. Liang, P. a. Ma, Z. Hou, Z. Cheng, J. Lin, *Adv. Funct. Mater.* **2017**, *27*, 1703535.
[57] T. Xuan, J. Huang, H. Liu, S. Lou, L. Cao, W. Gan, R.-S. Liu, J. Wang, *Chem. Mater.* **2019**, *31*, 1042.
[58] H.-R. Lou, Z.-Z. Ye, H.-P. He, *Acta Phys. Sin.* **2019**, *68*, 719.
[59] J. Chen, D. Liu, M. J. Al-Marri, L. Nuuttila, H. Lehtivuori, K. Zheng, *Sci. China Mater.* **2016**, *59*, 719.
[60] B. T. Diroll, G. Nedelcu, M. V. Kovalenko, R. D. Schaller, *Adv. Funct. Mater.* **2017**, *27*, 1606750.